The Astrophysical Journal, 626:396–410, 2005 June 10

X-RAY OBSERVATIONS OF THE BOUNDARY LAYER IN DWARF NOVAE AT LOW ACCRETION RATES

Dirk Pandel
Department of Physics, University of California, Santa Barbara, CA 93106;
dpandel@xmmom.physics.ucsb.edu

France A. Córdova
Institute of Geophysics and Planetary Physics, Department of Physics, University of California, Riverside, CA 92521

Keith O. Mason
Mullard Space Science Laboratory, Department of Space and Climate Physics, University College London, Holmbury St. Mary, Dorking, Surrey RH5 6NT, UK

and

William C. Priedhorsky
Los Alamos National Laboratory, International, Space, and Response Division, Mail Stop B241, Los Alamos, NM 87545
Received 2004 August 2; accepted 2005 March 1

ABSTRACT

We present a spectral analysis of *XMM-Newton* data of 10 dwarf novae, 9 of which were observed during a quiescent state. The X-ray spectra indicate the presence of a hot, optically thin plasma with a temperature distribution consistent with a simple, isobaric cooling flow. The likely origin of the X-ray emission is cooling plasma in the boundary layer settling onto the white dwarf. Using a cooling flow model, we derive the temperatures, accretion rates, rotational velocities, and elemental abundances of the X-ray–emitting gas. We discuss the implications of our findings for the structure of the boundary layer. A comparison of X-ray and ultraviolet luminosities finds no evidence of underluminous boundary layers in any of the quiescent dwarf novae. The X-ray spectrum of EI UMa differs significantly from those of the other objects, showing a strong fluorescent Fe Kα line and a strong O VII line triplet. Based on the observational evidence, we argue that EI UMa is most likely an intermediate polar and not, as previously thought, a dwarf nova.

Subject headings: accretion, accretion disks — binaries: close — novae, cataclysmic variables — stars: dwarf novae — stars: individual (OY Carinae, WW Ceti, AB Draconis, U Geminorum, VW Hydri, WX Hydri, T Leonis, TY Piscis Austrini, EI Ursae Majoris, SU Ursae Majoris) — X-rays: binaries

1. INTRODUCTION

Dwarf novae belong to the class of nonmagnetic cataclysmic variables in which the magnetic field of the white dwarf is too weak to disrupt the accretion disk, so that the disk can extend close to the surface of the white dwarf (see Warner 1995 for a review of dwarf novae). The material in the inner disk, initially moving with a Keplerian velocity, must dissipate its rotational kinetic energy in order to accrete onto the slowly rotating white dwarf. The structure of the boundary layer, i.e., the transition region between the disk and the white dwarf, is poorly understood, and theoretical modeling is complicated by the strong shearing and turbulence present in the accretion flow. A number of widely different models have been proposed, including a disk-like boundary layer (Narayan & Popham 1993), a coronal siphon flow (Meyer & Meyer-Hofmeister 1994), a spherical corona (Mahasena & Osaki 1999), and a hot settling flow (Medvedev & Menou 2002).

During their quiescent state, dwarf novae are copious sources of hard X-rays, with energies of 10 keV and higher. The origin of the X-ray emission is thought to be a hot, optically thin plasma in the boundary layer. Observations (e.g., of eclipse profiles) have shown that the X-ray–emitting region is generally small and close to the white dwarf's surface (e.g., van Teeseling et al. 1996; Mukai et al. 1997). Basic accretion theory predicts that half of the total accretion energy should emerge from the disk at optical and ultraviolet (UV) wavelengths, while the other half is released in the hot boundary layer as X-ray and extreme UV emission (Lynden-Bell & Pringle 1974). However, in many dwarf novae the X-ray luminosity is found to be lower than predicted (e.g., Ferland et al. 1982; van Teeseling & Verbunt 1994). It has been suggested that this "mystery of the missing boundary layers" may be due to a disruption of the inner disk caused by irradiation from the white dwarf (King 1997), evaporation of the inner disk via a coronal siphon flow (Meyer & Meyer-Hofmeister 1994), or white dwarfs rotating near breakup velocity (Ponman et al. 1995).

The greatly improved sensitivity and spectral resolution of the new generation of X-ray telescopes promises to reveal a much more detailed view of the boundary layer. In this paper, we present a spectral analysis of *XMM-Newton* data of 10 dwarf novae at low accretion rates. The high sensitivity of *XMM-Newton* enables us to examine the multitemperature nature of the boundary layer and derive the temperature distribution of the X-ray–emitting plasma. We compare X-ray and UV luminosities in order to investigate whether boundary layer luminosity is missing in any of the dwarf novae. Our spectral analysis further provides estimates of the accretion rates, boundary layer rotation velocities, and elemental abundances in the accreting material. We use our findings to draw conclusions about the structure of the boundary layer. Based on our X-ray spectral analysis, we argue that one of the objects, EI UMa, is actually an intermediate polar

TABLE 1
SYSTEM PARAMETERS

Object Name	P_{orb} (minutes)	D (pc)	Type	T_{ob} (days)	T_{sob} (days)	i (deg)	M_{wd} ($M_\odot$)	R_{wd} (10^8cm)
T Leo	84.7	92 ± 15[a]	SU	?	420	65 ± 19	0.4[b]	10.5
OY Car	90.9	86 ± 4[c]	SU	14	325	83.3 ± 0.2	0.685 ± 0.011	7.8
VW Hyi	107.0	65[d]	SU	28	183	60 ± 10	0.63 ± 0.15	8.3
WX Hyi	107.7	265[d]	SU	11	180	40 ± 10	0.90 ± 0.30	6.2
SU UMa	109.9	280[d]	SU	5–33	160	44[d]	0.7*	7.7
TY PsA	121.1	190[d]	SU	30–50	202	65[d]	0.7*	7.7
AB Dra	218.9	90[e]	ZC	8–22	...	40 ± 20[f]	0.7*	7.7
WW Cet	253.2	146 ± 25[a]	ZC[d]	45	...	54 ± 4	0.85 ± 0.11	6.5
U Gem	254.7	96.4 ± 4.6[g]	UG	132	...	69 ± 2	1.07 ± 0.08	4.9
EI UMa	386.1	100*	UG?	?	...	23[h]	0.95*	5.9

NOTES.—The system parameters shown are the orbital period P_{orb}, distance D, dwarf nova type (U Gem, SU UMa, or Z Cam), average time between outbursts T_{ob} and superoutbursts T_{sob}, orbital inclination i, white dwarf mass M_{wd}, and white dwarf radius R_{wd}. Unless noted otherwise, the parameters are from Ritter & Kolb (2003). Parameter values followed by an asterisk are not known and have been assumed (for M_{wd} of EI UMa, see § 4.7). The values of R_{wd} were derived from M_{wd} using the mass-radius relationship in Hamada & Salpeter (1961).
[a] From Sproats et al. 1996.
[b] From Shafter & Szkody 1984.
[c] From Bruch et al. 1996.
[d] From Warner 1987.
[e] From Wade 1982.
[f] From La Dous 1991.
[g] From Harrison et al. 1999.
[h] From Thorstensen 1986.

and not, as previously thought, a U Gem–type dwarf nova. We included in our sample the dwarf nova VW Hyi, for which we already presented a spectral and timing analysis of the *XMM-Newton* data in Pandel et al. (2003). The OY Car data has previously been presented in Ramsay et al. (2001a, 2001b) and Wheatley & West (2003). Some properties of the 10 cataclysmic variables in our sample are summarized in Table 1.

2. OBSERVATIONS AND DATA REDUCTION

We present X-ray and UV data obtained with *XMM-Newton* (Jansen et al. 2001) during 12 observations of 10 dwarf novae. Our analysis includes data from the EPIC MOS and PN cameras (Turner et al. 2001; Strüder et al. 2001), the RGS (den Herder et al. 2001), and the Optical Monitor (OM; Mason et al. 2001). A summary of the observations is given in Table 2. We derived the state of the binaries from light curves provided by the American Association of Variable Star Observers (AAVSO) and from the *B* magnitudes measured with the *XMM-Newton* OM. All but two of the observations occurred during quiescence. When known, we quote in the last column of Table 2 the number of days since the end of the last outburst. All of the SU UMa–type dwarf novae were observed after a normal outburst, and none after a superoutburst.

From the EPIC MOS and PN data, we extracted source photons using a circular aperture with a radius of 40″. We included

TABLE 2
SUMMARY OF *XMM-Newton* OBSERVATIONS

		Effective Exposure Times (ks)				X-Ray Count Rates (s^{-1}) (0.2–12 keV)			UV Flux at 290 nm		
Object Name	Start of Obs. (MJD)	MOS	PN	RGS	OM	MOS-1	MOS-2	PN	(mJy)	*B* Magnitude	State
T Leo	52,426.363	12.3	10.0	12.8	7.8	$1.09^{l,m}$	$1.18^{s,t}$	$3.86^{f,m}$	1.65	16.2	Q
OY Car	51,724.939	51.4*	48.9*	52.2*	8.4	$0.39^{f,m}$	$0.39^{f,m}$	$1.19^{f,m}$	0.68/0.94	...	Q 4
	51,763.327	13.7*	6.2*	13.0*	10.0	$0.20^{f,m}$	$0.20^{f,m}$	$0.59^{f,m}$	...	16.8/16.2	Q 42
VW Hyi	52,201.222	18.7	16.1	19.3	17.3	$0.67^{s,m}$	$0.71^{s,t}$	$2.41^{f,m}$	7.5/10.6	14.4/13.9	Q 22
WX Hyi	52,282.148	9.8*	7.5*	10.3*	12.9	$0.24^{l,m}$	$0.26^{s,t}$	$0.87^{f,m}$	17.7	13.1	O
SU UMa	52,399.717	13.8*	9.1*	11.1*	9.0	$2.19^{s,m}$	$2.31^{s,t}$	$6.95^{f,m}$	4.8	...	Q 8
TY PsA	52,241.792	12.6	10.0	13.2	11.6	$0.38^{f,m}$	$0.41^{s,t}$	$1.36^{f,m}$	1.00	16.6	Q
AB Dra	52,553.235	11.7	10.0	9.2*	...	$0.68^{f,m}$	$0.72^{s,t}$	$2.40^{f,t}$	...	...	Q 5
WW Cet	52,249.724	12.1	9.5	12.7	11.2	$1.36^{l,m}$	$1.41^{s,t}$	$4.50^{f,m}$	2.7	15.5	Q 20
U Gem	52,377.214	22.4	21.6	22.9	20.8	$0.93^{l,m}$	$0.97^{s,t}$	$3.32^{s,m}$	5.2	14.5	Q 50
EI UMa	52,404.462	7.4	4.5*	6.6*	7.5	$1.93^{l,m}$	$2.08^{s,t}$	$6.64^{f,m}$	4.1	14.8	Q
	52,580.859	9.9	8.2	10.0	8.5	$2.03^{l,m}$	$2.25^{s,t}$	$6.89^{f,m}$	5.9	14.2	I

NOTES.—The table summarizes *XMM-Newton* observing dates, effective exposure times for all instruments, average EPIC count rates, as well as UV fluxes (UVW1 filter) and *B* magnitudes obtained with the OM. An asterisk following the exposure times indicates that some part of the exposure has been excluded due to high background. The superscripts following the EPIC count rates indicate the window mode (f: full frame, l: large, s: small) and the filter (t: thin, m: medium). The OM light curves for OY Car and VW Hyi showed significant orbital variations, so we quote the low and high brightness levels (not considering the eclipse in OY Car). The last column shows the state of the systems (Q: quiescent, I: intermediate, O: outburst) as derived from AAVSO light curves and B magnitudes followed by the number of days since the end of the last outburst, when known.

in our analysis good photon events (FLAG = 0), with patterns 0–12 for MOS and 0–4 for PN. Background rates were estimated using larger regions on the same CCD as the source image (annular regions for MOS and off-center regions for PN) unless the EPIC cameras were operated in small-window mode. In this case, regions on other CCDs had to be used. Vignetting corrections appropriate for the selected regions were applied to all background rates. For some observations we excluded time periods with high background (indicated by an asterisk following the exposure times in Table 2). After this exclusion, average EPIC background rates in the energy range 0.2–12 keV were typically ~1% of the source count rate, with the exception of AB Dra (7%) and WX Hyi (5%). For our analysis of the RGS data, we used the first-order spectra only.

We derived the UV fluxes and *B* magnitudes in Table 2 from the data obtained with the OM. The OM was operated in fast mode which, in addition to images, provided individual photon arrival times inside a small window, with a time resolution of 0.5 s. With the exception of the OY Car observations, the OM was configured to perform one 1.2 ks exposure with the *B* filter followed by several longer exposures with the UVW1 filter (240–340 nm). Because of technical problems, the data for one or both filters were lost during the AB Dra and SU UMa observations. No fast-mode data were available for the U Gem observation, so we derived the *B*/UV brightness from the OM images. We extracted source photons using a circular aperture with a 5″ radius and corrected the count rates for the 81% enclosed energy fraction of this aperture. We adopted for a count rate of 1 s^{-1} in the UVW1 filter a flux conversion of 0.126 mJy (4.5×10^{-16} ergs cm^{-2} s^{-1} $Å^{-1}$) at 290 nm, which is appropriate for UV-bright objects.[1] In the *B* filter, a count rate of 1 s^{-1} corresponds to a magnitude of 19.27 (*XMM-Newton* Users' Handbook).[2] The background rates, which we estimated from the OM images, were typically ~1 s^{-1} (0.1 mJy) for the UVW1 filter and ~5 s^{-1} for the *B* filter. We corrected the count rates for coincidence losses using the method described in the *XMM-Newton* Users' Handbook. Coincidence losses of 10% are expected for count rates of ~50 s^{-1}, corresponding to 5 mJy in the UVW1 filter and a magnitude of 15.0 in the *B* filter. Because of the high count rates, the coincidence loss correction for the WX Hyi data is probably unreliable. For OY Car and VW Hyi, which show strong orbital variations, we quote in Table 2 the minimum and maximum brightness during the orbital cycle (excluding the eclipse in OY Car).

3. SPECTRAL ANALYSIS

The medium-resolution EPIC spectra and the high-resolution RGS spectra of the 10 dwarf novae are shown in Figures 1–3. We performed the spectral fitting with the XSPEC package version 11.2 (Arnaud 1996). For optimal fit results, we binned the EPIC and RGS spectra at one-third of the respective FWHM detector resolution. To account for the low number of counts per bin, we used C-statistic (Cash 1979) instead of χ^2-statistic. For clarity, the spectra in Figures 1–3 are shown with a lower resolution than was used for fitting.

The spectral fitting was performed simultaneously for the five spectra from the three EPIC cameras and the two RGS spectrometers. For the EPIC spectra we restricted the fitting to the energy range 0.2–12 keV. We found that individual fits to the three EPIC spectra yield slightly different results, which we attribute to discrepancies in the cross-calibration. The differences are mainly reflected in the spectral slopes (parameter α below), which may differ by up to 6 σ between the three EPIC spectra (see also our analysis of the VW Hyi data in Pandel et al. 2003). As a consequence, quality criteria for the simultaneous fits do not reflect how well the spectral models agree with the data but rather how well the different EPIC cameras agree with each other. We therefore used as a quality criterion the χ^2 for a fit to only the spectrum of the EPIC PN, the detector with the highest signal-to-noise ratio (S/N). In order to apply χ^2-statistic, we rebinned the data with a minimum of 20 counts per bin. The quoted fit parameters, however, were obtained from the combined fits to the EPIC and RGS spectra. Because of the lower sensitivity, the RGS data have only a small influence on the fit parameters responsible for the X-ray continuum. However, they do complement the EPIC spectra in the determination of elemental abundances from the emission-line strengths (see Pandel et al. 2003 for a comparison between the abundances in VW Hyi derived from the EPIC and the RGS spectra).

3.1. *Cooling Flow Model*

The X-ray spectra (Figs. 1–3) are rich in emission lines, indicating the presence of a hot, optically thin plasma. Most prominent are the H- and He-like emission lines of the abundant elements from N to Fe, as well as some of the Fe L-shell lines between 10 and 18 Å (0.7–1.3 keV). The presence of emission lines from many different elements is an indication that the X-ray–emitting plasma covers a wide range of temperatures. We first attempted to fit the spectra with one or more single-temperature plasma models. As the single-temperature model we used the MEKAL model in XSPEC, which describes an optically thin and collisionally ionized, isothermal plasma based on calculations by Mewe et al. (1985) and Liedahl et al. (1995). We found that for most spectra a one- or two-temperature model is inconsistent with the data. The only exceptions are the WX Hyi spectrum and the second OY Car spectrum. The likely reason for the good agreement is the low S/N of both spectra. For most of the other dwarf novae, however, the spectra are well fitted by three- or four-temperature MEKAL models. Exceptions are the first OY Car spectrum and both EI UMa spectra, which are inconsistent with any MEKAL-based, multitemperature model. We discuss these special cases further in §§ 3.2 and 3.3.

It is evident from the multiple plasma temperatures required in our fits that the X-ray–emitting gas has a wide range of temperatures. This is in agreement with earlier findings for quiescent dwarf novae (e.g., Ishida et al. 1996; Szkody et al. 2002; Perna et al. 2003). A continuous temperature distribution is expected for accreting gas that cools as it settles onto the white dwarf. An appropriate model to describe such a plasma is that of an isobaric cooling flow. In a simple cooling flow model, the emission measure EM at each temperature is proportional to the time the cooling gas remains at this temperature (i.e., the cooling time) and therefore inversely proportional to the bolometric luminosity (e.g., Mushotzky & Szymkowiak 1988). The differential emission measure for an isobaric cooling flow is given by

$$\left|\frac{d\mathrm{EM}}{dT}\right|_{\mathrm{c.f.}} = \frac{5}{2}k\frac{\dot{M}}{\mu m_p}\frac{n^2}{\varepsilon(T,n)}, \quad (1)$$

where $\dot{M}$ is the accretion rate, m_p the proton mass, μ the mean molecular weight (~0.6), n the particle density, and $\varepsilon(T, n)$ the

[1] See http://xmm.vilspa.esa.es/sas/documentation/watchout/uvflux.shtml.

[2] Available at http://xmm.vilspa.esa.es/external/xmm_user_support/documentation/uhb/index.html.

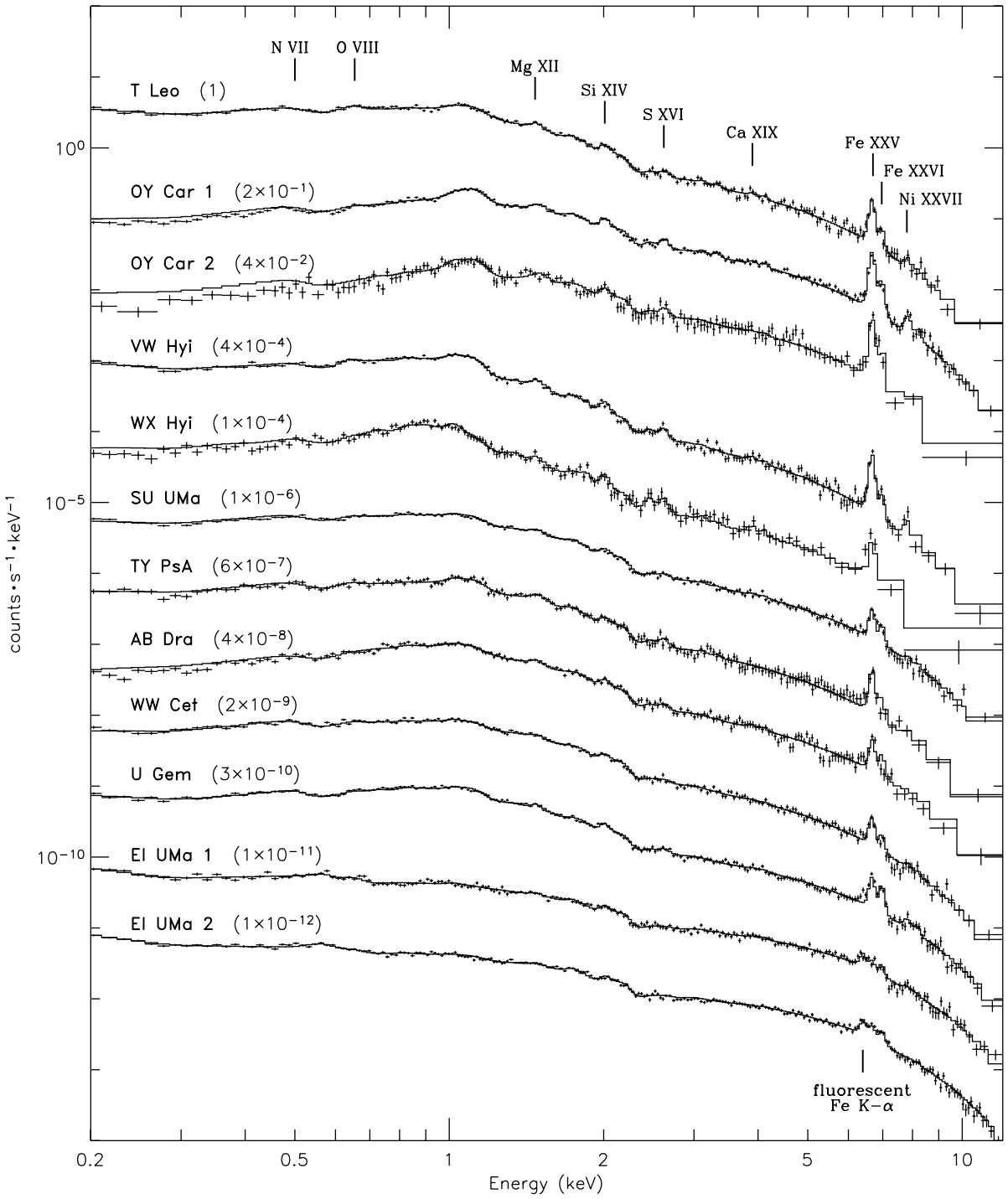

FIG. 1.—Combined EPIC MOS and PN spectra for the 12 observations of the 10 dwarf novae. The solid lines show the best fits with our cooling flow model (§ 3.1 and Table 3). For clarity, the spectra have been shifted vertically by the factors indicated in parentheses.

total emissivity per volume (in ergs s^{-1} cm^{-3}). This equation follows from the assumption that the plasma is cooling isobarically, i.e., the energy radiated by the plasma is $-5/2kdT$ per particle. Furthermore, it is assumed for this model that the plasma is optically thin, that any external input of energy (e.g., from the gravitational field) can be neglected, and that there is no heat conduction in the flow. Note that for a collisionally ionized plasma in thermal equilibrium $\varepsilon(T, n) \propto n^2$, so that the emission measure distribution is independent of the density and therefore independent of the geometry and scale of the cooling flow.

In XSPEC, a simple, isobaric cooling flow is described by the MKCFLOW model, which assumes the above emission measure distribution and calculates the X-ray spectrum at each temperature using the MEKAL model. The MKCFLOW model agrees with our data as well as the three- and four-temperature models described above. We find that small but statistically significant improvements over the MKCFLOW model can be achieved if the slope of the emission measure distribution is allowed to vary. Such deviations from an isobaric cooling flow could be caused by the strong gravitational field on the white dwarf, by the plasma becoming optically thick at lower temperatures, by heat conduction,

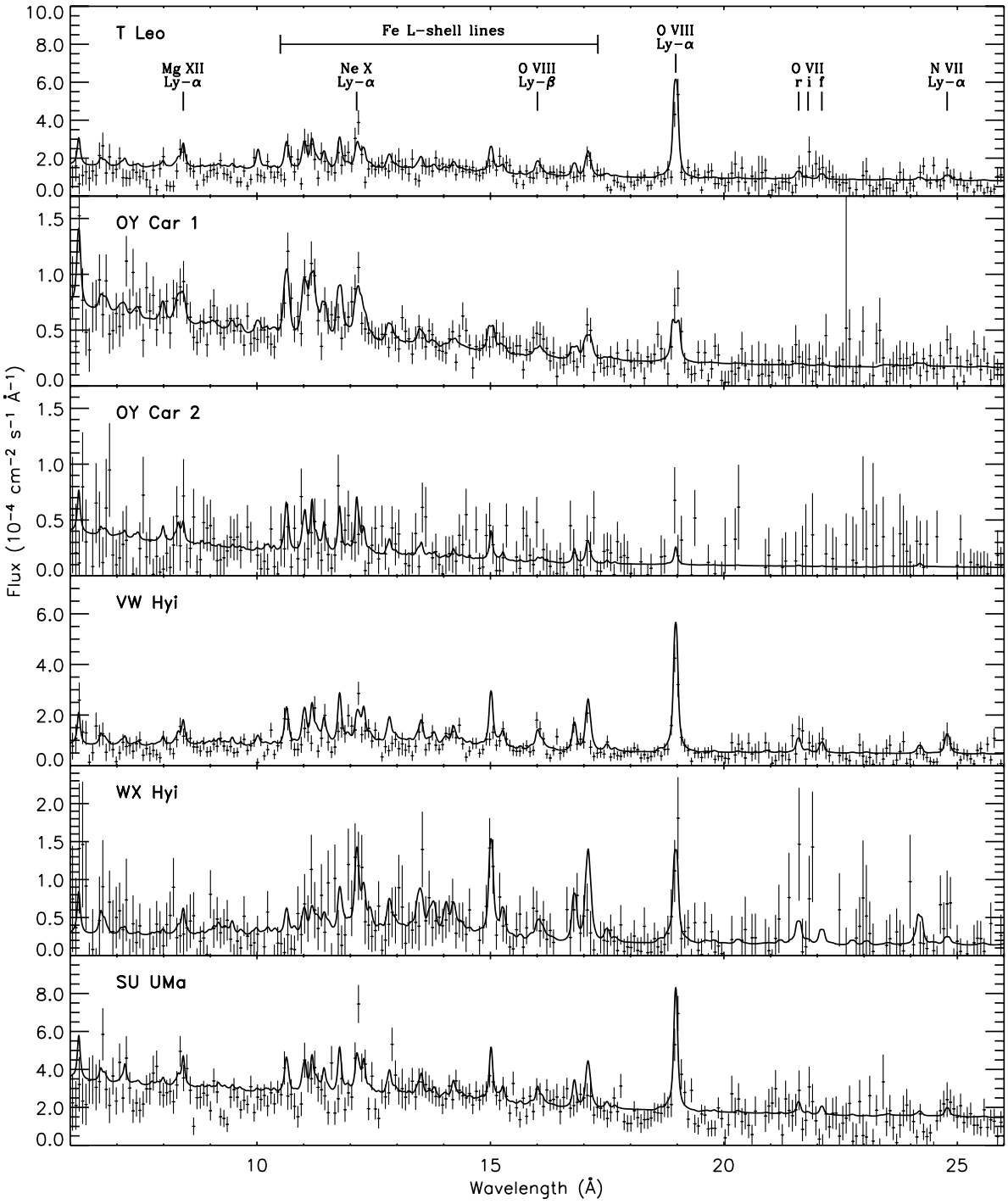

FIG. 2.—Flux-calibrated RGS spectra. The solid lines show the best fits with our cooling flow model (§ 3.1 and Table 3). The data are binned at approximately the FWHM detector resolution (0.07 Å).

or by uncertainties in the detector calibration. We modified the MKCFLOW model so that the emission measure distribution is given by

$$\frac{d\mathrm{EM}}{dT} = \left|\frac{d\mathrm{EM}}{dT}\right|_{\mathrm{c.f.}} \left(\frac{T}{T_{\max}}\right)^{\alpha}, \qquad (2)$$

where $T_{\max}$ is the initial temperature of the cooling gas, and α a power-law index that parameterizes the deviation from an isobaric flow. The other parameters in our model are the minimum temperature $T_{\min}$, the accretion rate $\dot{M}_{\mathrm{bl}}$ at $T_{\max}$ for a given distance, and the elemental abundances. We calculated the X-ray spectra by adding single-temperature MEKAL models on a grid with a spacing of 0.1 in $\log T$ between 8 eV and 80 keV. To determine the neutral hydrogen column density N_{H} of the intervening gas, we included photoelectric absorption in our model.

The resolution of the RGS spectra is sufficient to measure the rotational velocity of the boundary layer via Doppler broadening of emission lines. We therefore included line broadening in our model, assuming that the X-ray–emitting gas is a thin ring rotating with a nonrelativistic velocity and that half of the

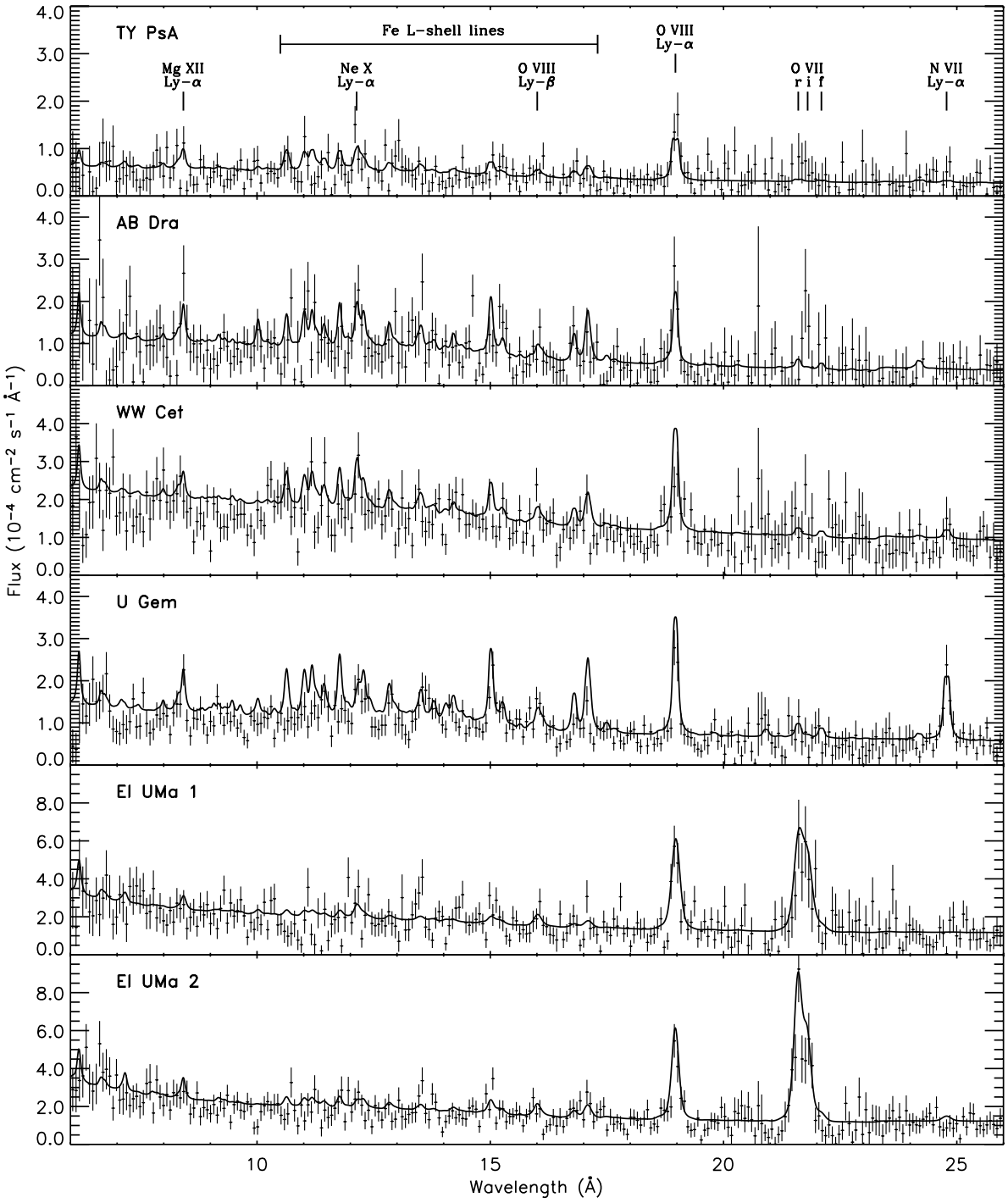

FIG. 3.—Flux-calibrated RGS spectra. The solid lines show the best fits with our cooling flow model (§ 3.1 and Table 3). The data are binned at approximately the FWHM detector resolution (0.07 Å).

ring is obscured by the white dwarf (i.e., the visible part is a semicircle). The line-broadening profile for an emission line at wavelength λ_0 is then given by

$$P(\lambda) = \pi^{-1}\left[(\beta_{\rm bl}\lambda_0)^2 - (\lambda - \lambda_0)^2\right]^{-1/2} \qquad (3)$$

for $|\lambda - \lambda_0| < \beta_{\rm bl}\lambda_0$, and $P(\lambda) = 0$ otherwise. Here $\beta_{\rm bl} = V_{\rm bl}\sin(i)/c$, with $V_{\rm bl}$ being the rotation velocity, i the orbital inclination, and c the speed of light.

The results of our fits with the cooling flow model are shown in Tables 3–5. The initial temperature $T_{\rm max}$ of the flow covers a wide range from 8 keV for VW Hyi to 55 keV for U Gem. We fixed the minimum temperature $T_{\rm min}$ at the lower bound of our model (8 eV) because preliminary fits showed that the parameter converges in all cases to this value. The upper limits on $T_{\rm min}$ derived from those fits are $\sim$200 eV for all objects (at 90% confidence level). This is consistent with the accreting gas not becoming optically thick before it has cooled to the low white dwarf temperature. In most cases, the parameter α is near 0, demonstrating that the emission measure distributions are close to that of the simple cooling flow model (eq. [1]). Only for WX Hyi, which was observed during outburst, does α indicate a significant

TABLE 3
Fit Parameters for the Cooling Flow Model

Object	kT_{max} (keV)	α	$\dot{M}_{bl}$ ($\times 10^{-12}$ $M_\odot$ yr^{-1})	N_H ($\times 10^{20}$ cm^{-2})	$V_{bl} \sin i$ (km s^{-1})	L_{bl} ($\times 10^{31}$ ergs s^{-1})	χ^2 (dof) for PN	Prob. (%)
T Leo.....	10.8 ± 0.8	0.19 ± 0.09	13 ± 2	0.3 ± 0.2	710^{+240}_{-380}	3.0	204 (180)	11
OY Car.....	11.7 ± 0.9	0.35 ± 0.07	6.8 ± 0.7	2.8 ± 0.3	1350^{+400}_{-400}	1.5	305 (211)	0
	11.0 ± 0.3	0.26 ± 0.07	4.0 ± 0.1	2.9 ± 0.6	250^{+700}_{-250}	0.84	93 (100)	68
VW Hyi.....	8.2 ± 0.3	-0.05 ± 0.06	3.7 ± 0.4	$0.0 + 0.05$	580^{+240}_{-250}	0.81	181 (171)	29
WX Hyi.....	26.8 ± 3.2	-0.72 ± 0.05	3.4 ± 0.7	2.3 ± 0.4	720^{+310}_{-330}	7.1	82 (95)	82
SU UMa.....	19.3 ± 1.8	0.07 ± 0.06	140 ± 20	1.2 ± 0.2	430^{+270}_{-430}	66.0	256 (215)	3
TY PsA	10.8 ± 0.6	0.37 ± 0.07	25 ± 5	1.5 ± 0.3	1100^{+500}_{-500}	4.8	143 (142)	45
AB Dra.....	21.6 ± 1.8	-0.18 ± 0.05	3.7 ± 0.6	6.1 ± 0.4	660^{+400}_{-660}	2.5	217 (196)	15
WW Cet	14.9 ± 1.1	0.24 ± 0.09	35 ± 5	2.1 ± 0.3	800^{+460}_{-470}	10.7	215 (192)	12
U Gem.....	55 ± 10	-0.23 ± 0.05	2.6 ± 0.4	0.5 ± 0.2	730^{+220}_{-210}	4.9	246 (209)	4
EI UMa	50 ± 5	0.05 ± 0.05	13.0 ± 0.6	0.7 ± 0.4	...	17.4	237 (241)	56
	54 ± 5	-0.03 ± 0.05	12.6 ± 0.7	1.3 ± 0.2	...	19.8	339 (241)	0

Notes.—The table shows the fit results for our cooling flow model described in § 3.1. $\dot{M}_{bl}$ and L_{bl} were derived using the distances in Table 1 and with the assumption that half of the beltlike boundary layer is obscured by the white dwarf. The uncertainties represent the 90% confidence level. Note that the values for χ^2 and the null hypothesis probability shown in the last two columns represent the fit quality for the EPIC PN spectra only, whereas the fit parameters were obtained from combined fits to all EPIC and RGS spectra (see § 3). Additional fit parameters for OY Car and EI UMa are shown in Table 4.

deviation from a simple cooling flow. The apparently good quality of the fit is likely a result of the low S/N of the WX Hyi data. To calculate the accretion rates $\dot{M}_{bl}$ and the unabsorbed luminosities L_{bl}, we used the distances shown in Table 1 and assumed that half of the beltlike boundary layer is obscured by the white dwarf. We further assumed isotropic emission and neglected reflection of X-rays off the white dwarf. Since typically ~70% of the flux is emitted in the 0.2–12 keV energy range and directly detected by *XMM-Newton*, the estimate of L_{bl} is fairly model independent.

For most of the dwarf novae, we find significantly nonzero boundary layer rotation velocities $V_{bl} \sin i$. However, all velocities are considerably smaller than the Keplerian velocity near the white dwarf's surface (~3000 km s^{-1}). The line broadening caused by the orbital motion of the white dwarf itself is of order 100 km s^{-1} and can be neglected. Note that the resolution of the EPIC spectra is insufficient to resolve any Doppler broadening. The rotation velocities are therefore solely constrained by the emission lines in the RGS spectra, in particular the strong O VIII Kα line. We found that fits to only the O VIII Kα line yield similar results as the global fits, albeit with slightly larger uncertainties.

The low values for χ^2 demonstrate that the X-ray spectra are well described by our cooling flow model. As mentioned earlier, the χ^2-values in Table 3 represent the fit quality for the EPIC PN spectra only, while the fit parameters were obtained from combined fits to all EPIC and RGS spectra. Using the χ^2 of the EPIC PN spectra as a quality measure was necessary to avoid the bias from the cross-calibration discrepancies between the instruments. The elemental abundances relative to their solar values are shown in Table 5. We obtained very good constraints for the abundances of O and Fe. Not shown are the abundances for Na, Al, Ar, Ca, and Ni, which are included in the MEKAL model but for which the fit did not provide useful constraints.

3.2. *OY Car*

The spectrum of OY Car is qualitatively similar to those of the other dwarf novae in our sample. The only apparent difference is the lower flux at low energies, which may indicate intrinsic absorption. OY Car, being the only eclipsing system in our sample, has a high orbital inclination (83°), and it is likely that some of the boundary layer emission is absorbed by the accretion disk. We therefore included in our model absorption by a partially covering, neutral absorber (PCFABS model in XSPEC). This additional model component significantly improved the quality of the fit. The best-fitting parameters for the partial absorber component are shown in Table 4.

For the first of the two OY Car observations, the somewhat large $\chi^2_{red} = 1.45$ for the PN spectrum seems to indicate a disagreement with our model. However, we find that the combined MOS spectra are in very good agreement with our model, with $\chi^2_{red} = 455/425 = 1.07$ (null hypothesis probability 15%). A comparison among the three EPIC spectra showed that below 0.5 keV the measured flux in the PN spectrum is ~10% lower than in the MOS spectrum. We therefore suspect that the large

TABLE 4
Additional Fit Parameters

	Partial Absorber			Blackbody		Equivalent Line Widths (eV)			
Object	N_H (10^{21}cm^{-2})	Covering Fraction	Doppler Width σ_v (km s^{-1})	kT_{bb} (eV)	Area (km^2)	O VII r (21.6 Å)	O VII i (21.8 Å)	O VII f (22.1 Å)	Fe Kα (6.4 keV)
OY Car.....	9.9 ± 1.2	0.49 ± 0.03	...	...	...	...	...	...	...
	9.7 ± 1.0	0.58 ± 0.02	...	...	...	...	...	...	...
EI UMa	36 ± 5	0.43 ± 0.02	1140^{+730}_{-300}	50 ± 5	13 ± 9	15 ± 5	12 ± 5	<3	97 ± 27
	35 ± 4	0.49 ± 0.03	900^{+340}_{-320}	52 ± 5	19 ± 13	20 ± 4	12 ± 4	<2	118 ± 21

Note.—Additional parameters for our model fits to the spectra of OY Car (§ 3.2) and EI UMa (§ 3.3).

TABLE 5
Elemental Abundances

Object	C	N	O	Ne	Mg	Si	S	Fe
T Leo	0.6 ± 0.8	0.9 ± 0.9	0.79 ± 0.12	0.5 ± 0.3	1.0 ± 0.4	0.9 ± 0.2	0.5 ± 0.3	0.72 ± 0.07
OY Car	2.2 ± 1.1	0.0 + 0.9	0.53 ± 0.12	0.8 ± 0.3	0.8 ± 0.4	1.4 ± 0.2	1.3 ± 0.3	1.57 ± 0.08
	1.1 ± 1.7	0.0 + 0.7	0.30 ± 0.25	1.1 ± 0.9	1.1 ± 0.9	1.1 ± 0.6	1.2 ± 0.7	1.48 ± 0.17
VW Hyi	1.0 ± 0.6	1.5 ± 1.0	0.82 ± 0.10	0.3 ± 0.3	1.1 ± 0.3	1.2 ± 0.2	1.1 ± 0.3	1.01 ± 0.06
WX Hyi	1.3 ± 0.7	0.9 ± 1.0	0.48 ± 0.12	1.2 ± 0.5	1.1 ± 0.6	1.9 ± 0.5	2.3 ± 0.7	0.85 ± 0.09
SU UMa	1.2 ± 0.6	0.4 ± 0.6	0.41 ± 0.08	0.3 ± 0.2	0.7 ± 0.3	0.8 ± 0.2	0.3 ± 0.3	0.58 ± 0.06
TY PsA	0.1 ± 1.1	0.3 ± 1.7	0.62 ± 0.18	0.4 ± 0.5	1.1 ± 0.5	0.7 ± 0.3	0.9 ± 0.5	0.69 ± 0.08
AB Dra	1.1 ± 0.7	0.0 + 0.3	0.28 ± 0.08	0.2 ± 0.2	0.7 ± 0.3	0.6 ± 0.2	0.5 ± 0.3	0.45 ± 0.05
WW Cet	0.4 ± 0.5	0.4 ± 0.9	0.37 ± 0.09	0.4 ± 0.3	0.5 ± 0.3	0.6 ± 0.2	0.2 ± 0.3	0.43 ± 0.05
U Gem	0.0 + 0.4	5.1 ± 1.3	0.72 ± 0.11	0.1 ± 0.4	1.5 ± 0.5	1.7 ± 0.3	0.8 ± 0.4	1.40 ± 0.10
EI UMa	2.2 ± 1.6	0.0 + 1.8	1.30 ± 0.25	0.5 ± 0.4	1.0 ± 0.6	1.6 ± 0.5	0.0 + 0.7	0.36 ± 0.08
	1.0 ± 1.3	0.6 ± 1.6	1.00 ± 0.19	0.1 ± 0.3	1.3 ± 0.5	1.2 ± 0.4	0.0 + 0.3	0.45 ± 0.07

Notes.—The table shows the elemental abundances obtained from our cooling flow model (§ 3.1). Abundances are given relative to the solar values in Anders & Grevesse (1989). The uncertainties represent the 90% confidence level.

χ^2 in Table 3 is a result of calibration uncertainties of the PN detector. OY Car is the only object in our sample that was observed early on during the *XMM-Newton* mission when instrument calibration was still at an early stage. We also found discrepancies between the RGS and EPIC data at low energies. Below 0.5 keV, the RGS measured more than double the flux seen with the EPIC detectors. This discrepancy is the reason why our model fits for OY Car appear to overpredict the EPIC flux at low energies (see Fig. 1).

We conclude that the spectrum of OY Car is in good agreement with our cooling flow model provided that partial absorption by the accretion disk is considered. In our model fits we used a simple partial absorber with a single column density and covering fraction. In reality, absorption by the disk is likely more complex, with a continuously varying column density. However, the quality of our data is insufficient to fit models with multiple partial absorbers.

3.3. *EI UMa*

The spectrum of EI UMa is qualitatively very different from those of the other objects in our sample. The most noticeable differences are the harder spectral slope, the weakness of Fe L-shell emission at 0.7–1.3 keV, the fluorescent Fe Kα line at 6.4 keV, and the strong O VII triplet at 22 Å. These spectral features are not typical for dwarf novae, but they suggest that EI UMa is a magnetic system of the intermediate polar type. We will discuss this hypothesis further in § 4.7. For the purpose of spectral fitting, we assume in this section that EI UMa is an intermediate polar.

The accretion disk in intermediate polars is disrupted at some radius by the magnetic field of the white dwarf, and the disk material is funneled along the field lines onto the magnetic poles. At some height above the white dwarf, the supersonic accretion flow forms a standoff shock that heats the gas to temperatures in excess of 10^8 K. Below the shock, the hot plasma is compressed as it piles up on the white dwarf, and it begins to cool via the emission of X-rays. A recent review of the standard model for accretion onto magnetic white dwarfs is given in Wu (2000).

We modeled the X-ray emission from the accretion column using the same cooling flow model as for the dwarf novae (see § 3.1). In intermediate polars, reflection of X-rays by the white dwarf slightly increases the observed flux above ~5 keV. We therefore included a simple multiplicative reflection model (HREFL in XSPEC), in which we assumed an angle of 30° between the line of sight and the surface normal. Note that the contribution from reflection is fairly small (~20% at 10 keV), and the use of a simple reflection model is sufficient. The assumed reflection angle has only a small impact on our fit results, and changing the angle to 60° only increases the two parameters of the partial absorber component by ~5%. Partial absorption of X-rays by the cooler preshock flow is observed in many intermediate polars. Adding a partially covering, neutral absorber (PCFABS in XSPEC) to our model significantly improved the quality of the fit. The partial absorber was applied only to the cooling flow and none of the other components.

The cooling flow model does not account for the strong Fe Kα line at 6.4 keV and the O VII line triplet at 22 Å. We therefore included these lines individually in our model. The Fe Kα line is likely caused by fluorescence in the cooler preshock flow or the photosphere of the white dwarf. The observed flux in the energy range 0.2–0.3 keV is higher than predicted by the cooling flow model. This flux excess is likely the high-energy tail of the thermal emission from the white dwarf's photosphere below the accretion column. To account for this excess, we added a single-temperature blackbody component to our model. We further included Doppler broadening with a Gaussian line profile.

The fit results for our model are shown in Tables 3 and 4. The parameter α is near zero, indicating that the postshock flow is close to a simple, isobaric cooling flow. The high plasma temperature $kT_{\max} \approx 50$ keV is probably responsible for the harder spectral slope compared to the dwarf novae. The strong continuum emission from the high-temperature plasma considerably reduces the equivalent widths of lines predominantly emitted by the cooler plasma in the accretion column. This may explain the apparent weakness of the Fe L-shell lines. We find that about half of the X-ray–emitting region is obscured by a neutral absorber with a large column density of $\sim 4 \times 10^{22}$ cm^{-2}. To calculate the total accretion rate $\dot{M}_{\rm bl}$ and luminosity $L_{\rm bl}$, we assumed that one of the two accreting poles is obscured by the white dwarf. The given $L_{\rm bl}$ is the unabsorbed luminosity of the cooling flow component only.

The temperature of the blackbody component (~50 eV) is at the high end of the temperature range observed in intermediate polars (e.g., Haberl & Motch 1995; de Martino et al. 2004). The fractional emitting area of the blackbody $f_{\rm eff} \approx 3 \times 10^{-8}$ is very small, considerably smaller than the typical size of the accretion region $f_{\rm zone} \approx 10^{-4}$ to 10^{-3}. However, it is possible that $f_{\rm eff} \ll f_{\rm zone}$ if accretion is very inhomogeneous and occurs via

dense filaments or blobs (Hameury & King 1988). Blackbody emission with a similarly small effective area $f_{\rm eff}$ has been observed in the X-ray spectra of several other intermediate polars (Haberl et al. 2002; de Martino et al. 2004). Note that the bolometric luminosity of the blackbody component is only $\sim$0.5% of the cooling flow luminosity $L_{\rm bl}$. This suggests that considerably more blackbody radiation is emitted from a larger area at lower temperatures and that our X-ray spectra only show emission from the hottest parts of the accretion region.

Our model is in excellent agreement with the spectrum from the first EI UMa observation. For the second observation, however, the model does not provide a good fit. This is surprising as there are no apparent differences between the two observations other than a slight difference in the X-ray and optical brightness. We suspect that, during the second observation, absorption by the preshock accretion flow was more complex than the simple partially covering, neutral absorber in our model. Some improvement of the fit could be achieved by adding a second partial absorber to the model. This may indicate a continuous distribution of column densities. It is also possible that the absorbing material is partially ionized and the neutral absorber model is insufficient. The differences between the two spectra may simply be a result of phase-dependent absorption. However, our knowledge of the white dwarf spin period and the binary orbital period is insufficient to compare the spin and orbital phases for the two observations.

4. DISCUSSION

Our sample of nine dwarf novae allows us to investigate some general properties of dwarf novae at low accretion rates (10^{-12} to $10^{-10}\ M_\odot\ {\rm yr}^{-1}$). All of the dwarf novae, except WX Hyi, were observed during their quiescent state. Even though WX Hyi was in outburst, its luminosity was lower than for some of the quiescent dwarf novae. EI UMa, which is most likely an intermediate polar, is discussed separately in § 4.7.

4.1. *X-Ray/UV Luminosities and the Missing Boundary Layers*

Basic accretion theory predicts that roughly half of the gravitational energy of the accreting matter is released by the disk as optical and UV radiation. For white dwarfs rotating much slower than their breakup velocity, the other half should be liberated as X-rays in the boundary layer, where the disk material is decelerated from its Keplerian velocity to the rotation velocity of the white dwarf (e.g., Lynden-Bell & Pringle 1974). It is therefore expected that the disk luminosity $L_{\rm disk}$ and the boundary layer luminosity $L_{\rm bl}$ are roughly equal. However, observations have shown that the X-ray luminosity is actually lower than predicted, which has become known as the "mystery of the missing boundary layers" (e.g., Ferland et al. 1982; van Teeseling & Verbunt 1994). In this section we investigate whether the boundary layers are underluminous for the eight quiescent dwarf novae in our sample.

Figure 4 shows the boundary layer luminosity $L_{\rm bl}$ derived from the X-ray spectrum versus the spectral luminosity at 290 nm $L_{\rm UVW1}$ obtained from the OM data. No OM data were available for AB Dra, so we assumed a flux of 9 mJy, which we derived by scaling the spectrum in Verbunt (1987) to match the visual magnitude in the AAVSO light curve at the time of the *XMM-Newton* observation ($V = 14.3$). The solid and dotted lines in Figure 4 show the $L_{\rm UVW1}$ that is expected if $L_{\rm disk} = L_{\rm bl}$. Here we derived $L_{\rm UVW1}$ from $L_{\rm disk}$ using a blackbody disk model (e.g., Mitsuda et al. 1984; Makishima et al. 1986). The model requires only two parameters, the inner disk radius $R_{\rm in}$ and the blackbody temperature at $R_{\rm in}$. Our predictions are shown for $R_{\rm in} = 5000$ km (*solid line*) and 10,000 km (*dotted line*), which is appropriate for white dwarf masses $M_{\rm wd} = 1.1\ M_\odot$ and $0.45\ M_\odot$, respectively (assuming that $R_{\rm in} = R_{\rm wd}$). Note that $M_{\rm wd}$ and $R_{\rm in}$ have only a small impact on the predicted $L_{\rm UVW1}$.

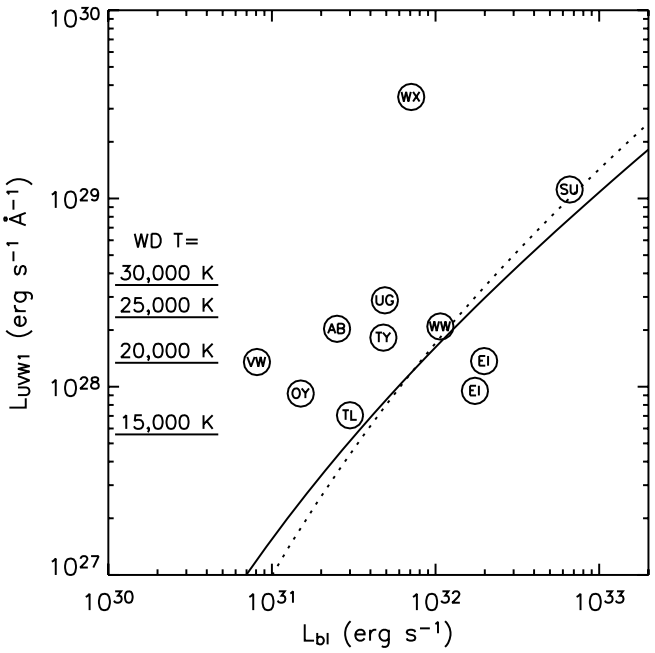

FIG. 4.—Boundary layer luminosity derived from the X-ray spectrum vs. UV spectral luminosity at 290 nm measured with the OM (see § 4.1). The solid and dotted lines show the UV luminosity predicted by a simple accretion disk model for two inner disk radii $R_{\rm in} = 5000$ km (*solid line*) and $R_{\rm in} = 10{,}000$ km (*dotted line*). The short horizontal lines show the UV luminosity of a white dwarf with radius $R_{\rm wd} = 8000$ km at various temperatures.

For all dwarf novae in our sample, the observed $L_{\rm UVW1}$ shown in Figure 4 is at least equal to or larger than the value expected if $L_{\rm disk} = L_{\rm bl}$. Only the probable intermediate polar EI UMa has a lower UV luminosity, which is consistent with the truncation of the disk by the magnetic field (see § 4.7). The highest $L_{\rm UVW1}$ was found for WX Hyi, which was observed during outburst. The UV luminosity in WX Hyi was probably enhanced because of a high disk accretion rate.

The diamond symbols in Figure 5 show the ratio $L_{\rm disk}/L_{\rm bl}$ for the eight quiescent dwarf novae. The ratio was derived with the assumption that the observed UV flux is entirely due to the disk. We estimated $L_{\rm disk}$ from $L_{\rm UVW1}$ using the blackbody disk model described above. Here we assumed that $R_{\rm in} = R_{\rm wd}$. Note that, even though accretion rates are fairly low, the blackbody disk model describes the spectrum sufficiently well for our purposes. While the outer parts of the disk may be optically thin, the inner regions, where most of the accretion energy is released, are optically thick. The calculations by Tylenda (1981) show that, for the accretion rates considered here, the optical and UV continuum emission is well approximated by a blackbody disk model. Emission or absorption lines do not significantly affect our results, since no major lines lie in the UVW1 bandpass.

The above derivation of $L_{\rm disk}$ does not take into account the white dwarf emission, which can be a major contributor to the UV flux. The horizontal lines in Figure 4 show the UV spectral luminosity of a white dwarf at various temperatures. To correct our estimates of $L_{\rm disk}$, we assumed that the white dwarf radiates like a blackbody and subtracted the white dwarf emission from $L_{\rm UVW1}$, assuming a reasonable range of surface temperatures.

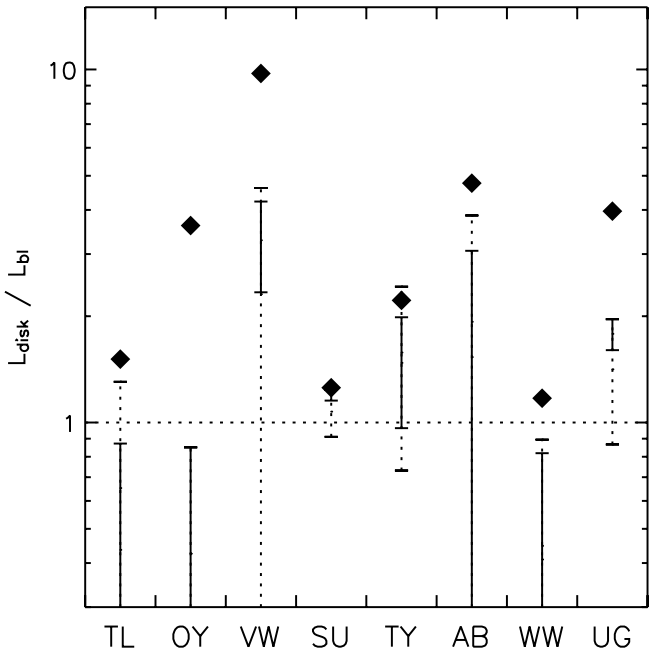

FIG. 5.—Ratio of disk luminosity to boundary layer luminosity for the eight quiescent dwarf novae in our sample (see § 4.1). The diamond symbols show $L_{\rm disk}/L_{\rm bl}$ when all of the UV flux observed with *XMM-Newton* is attributed to the disk. Corrected luminosity ratios taking into account the UV emission from the white dwarf are shown as solid bars for a reasonable range of surface temperatures. The dotted vertical bars indicate how the possible range would be extended if the disk were truncated at a radius up to $3R_{\rm wd}$.

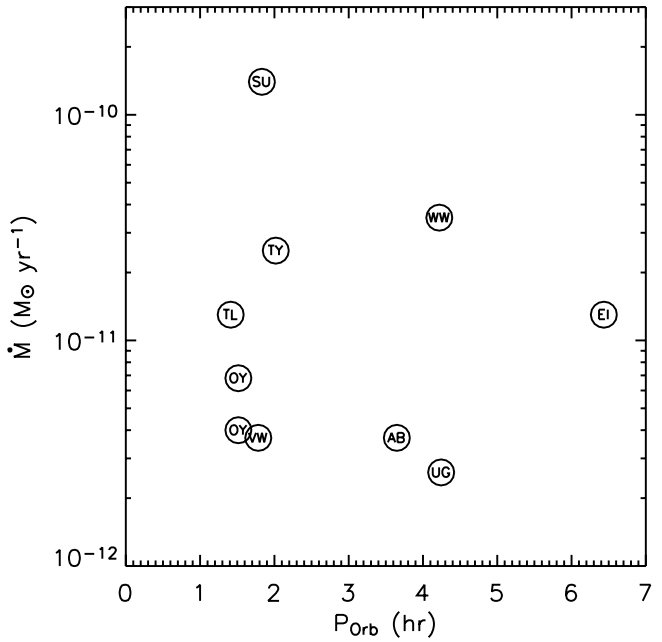

FIG. 6.—Boundary layer accretion rates vs. orbital periods for the quiescent objects in our sample.

To calculate the visible emitting areas, we used the white dwarf radii and orbital inclinations shown in Table 1 and assumed that the surface below the equator is obscured by the disk. For three of the dwarf novae, white dwarf temperatures have previously been measured, and we adopted the following temperature ranges, which are appropriate for the number of days since the last outburst: 13,000–18,000 K for OY Car (Hessman et al. 1989; Horne et al. 1994), 18,000–20,000 K for VW Hyi (Gaensicke & Beuermann 1996), and 31,000–34,000 K for U Gem (Long et al. 1994). For the dwarf novae without known white dwarf temperatures, we selected typical ranges based on the distribution in Sion (1991, 1999): 12,000–20,000 K for orbital periods below the 2–3 hr gap (T Leo, SU UMa, and TY PsA) and 20,000–40,000 K for periods above the gap (AB Dra and WW Cet).

The corrected $L_{\rm disk}/L_{\rm bl}$ ratios, obtained after subtracting the white dwarf emission, are shown in Figure 5 as solid vertical bars. For six of the dwarf novae, the allowed range is consistent with $L_{\rm disk} \approx L_{\rm bl}$. Only for VW Hyi and U Gem does $L_{\rm disk}/L_{\rm bl}$ appear to be notably above 1. It has been suggested that the disk in quiescent dwarf novae is truncated at a radius larger than $R_{\rm wd}$ (e.g., King 1997; Lasota et al. 1995). Truncation of the disk would impact our estimates of $L_{\rm disk}$ because it changes the parameter $R_{\rm in}$ of the disk model and the fraction of the white dwarf's surface obscured by the disk. The dotted vertical bars in Figure 5 show how the allowed range of $L_{\rm disk}/L_{\rm bl}$ would be extended if the disk were truncated somewhere between $R_{\rm wd}$ and $3R_{\rm wd}$. The extended ranges for VW Hyi and U Gem are now also consistent with $L_{\rm disk} \approx L_{\rm bl}$. Note, however, that in a truncated disk less gravitational energy is available, and one might expect that $L_{\rm disk}/L_{\rm bl} < 1$.

We conclude that the X-ray and UV emission from the eight quiescent dwarf novae is consistent with $L_{\rm disk} \approx L_{\rm bl}$ if the white dwarf emission and a possible truncation of the disk are taken into account. An excess of disk emission can be ruled out for four dwarf novae (T Leo, OY Car, SU UMa, and WW Cet), though an excess of boundary layer luminosity is possible for three of them. For the other four dwarf novae (VW Hyi, TY PsA, AB Dra, and U Gem), an underluminous boundary layer may be present, but the $L_{\rm disk}/L_{\rm bl}$ ratio can be at most 2–4. It is evident that in quiescent dwarf novae the problem of the underluminous boundary layers, if it exists at all, is much less pronounced than in dwarf novae during outburst.

4.2. *Accretion Rates during Quiescence*

Figure 6 shows the boundary layer accretion rates versus the orbital periods for the quiescent objects in our sample. The accretion rates cover a range of almost 2 orders of magnitude. The scatter of data points is similar to that found by Warner (1987) for the absolute visual magnitudes of the accretion disks in dwarf novae at minimum light. A correlation with the orbital period or the outburst interval as found by Warner (1987) is not apparent in our data. Note that accretion rates derived from the X-ray spectrum are fairly reliable and, unlike those estimated from the disk luminosity, do not require a detailed understanding of the disk physics or knowledge of the orbital inclination.

4.3. *Boundary Layer Rotation Velocities*

Figure 7 shows the ratio of the boundary layer rotation velocities $V_{\rm bl}$ (derived from $V_{\rm bl} \sin i$ in Table 3) and the Keplerian velocities at the white dwarf radius $V_{\rm Kepler} = (GM_{\rm wd}/R_{\rm wd})^{1/2}$. Note that the error bars in Figure 7 only include the uncertainty of the measured $V_{\rm bl} \sin i$ and not that of i or $V_{\rm Kepler}$. Since approximately $V_{\rm Kepler} \propto M_{\rm wd}^{0.9}$, the uncertainty of $V_{\rm bl}/V_{\rm Kepler}$ is somewhat larger for systems with poorly known white dwarf masses.

It is evident from Figure 7 that, for all dwarf novae in our sample, the boundary layer rotates considerably slower than the inner accretion disk. Note, however, that the measured $V_{\rm bl}$ depends mostly on the width of the O VIII Kα line and is therefore an estimate of the rotation velocity of the cooler gas in the lower parts of the boundary layer. In a cooling flow with $kT_{\rm max} = 20$ keV, half of the O VIII line flux is emitted at plasma

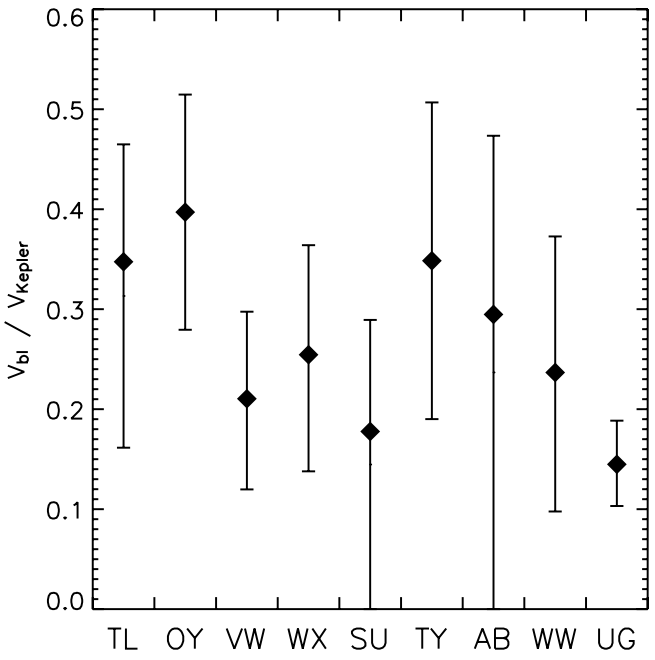

FIG. 7.—Ratio of boundary layer rotation velocity V_{bl} and Keplerian velocity V_{Kepler} at the white dwarf radius for the nine dwarf novae in our sample (see § 4.3). Error bars have been derived from the 90% confidence ranges of $V_{bl} \sin i$ in Table 3 and do not include the uncertainties of i and V_{Kepler}.

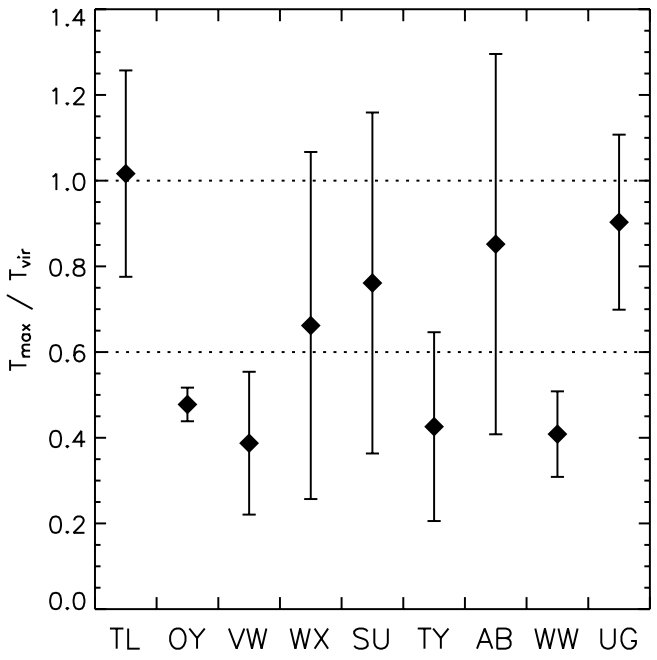

FIG. 8.—Ratio of initial cooling flow temperature T_{max} and virial temperature T_{vir} for the nine dwarf novae in our sample (see § 4.4). The two horizontal lines indicate ratios of 1 and $\frac{3}{5}$, respectively. Error bars show the 90% confidence range of T_{max} combined with the uncertainty of the white dwarf mass M_{wd}. For systems without known masses (SU UMa, TY PsA, AB Dra), we assumed $M_{wd} = 0.7 \pm 0.2\ M_{\odot}$, and for T Leo $M_{wd} = 0.4 \pm 0.05\ M_{\odot}$.

temperatures below 2 keV. The white dwarf rotation velocity V_{wd} is likely lower than the rotation velocity of the boundary layer, and V_{bl} can be considered an upper limit on V_{wd}. Consequently, all dwarf novae in our sample contain a white dwarf that is rotating considerably below the breakup velocity V_{Kepler}.

White dwarf rotation velocities have been measured for three objects in our sample. In VW Hyi, the white dwarf is rotating with a projected velocity $V_{wd} \sin i = 400-500$ km s^{-1} (Sion et al. 2001), which is close to our measurement of the boundary layer velocity $V_{bl} \sin i \approx 580$ km s^{-1}. In contrast, the upper limits on $V_{wd} \sin i$ of $\leq$100 km s^{-1} for U Gem (Sion et al. 1994) and $<$200 km s^{-1} for OY Car (Cheng et al. 1994) are significantly smaller than the boundary layer velocities of $\sim$730 and $\sim$1350 km s^{-1}, respectively. It is apparent that a high V_{bl} does not necessarily imply a high V_{wd}, and V_{wd} for the other dwarf novae could be anywhere in the range $0-V_{bl}$.

4.4. *Cooling Flow Temperatures*

The initial cooling flow temperatures T_{max} of the nine dwarf novae cover a wide range, from $\sim$8 keV for VW Hyi to $\sim$55 keV for U Gem with most temperatures concentrated around 10–20 keV (Table 3). The exceptionally high temperature in U Gem is likely a result of the larger white dwarf mass.

In Figure 8 we compare T_{max} to the virial temperature T_{vir} at the white dwarf radius. T_{vir} is the temperature that the disk material would have if all the kinetic energy from its Keplerian motion were instantly converted into heat. The virial temperature is given by $3/2kT_{vir} = 1/2\mu m_p V^2_{Kepler}$, where m_p is the proton mass and μ the mean molecular weight ($\sim$0.6). Since this equation gives the maximum energy per particle that can be dissipated, the temperature in the boundary layer cannot exceed T_{vir}. Indeed, $T_{max} \leq T_{vir}$ appears to be satisfied for our sample of dwarf novae.

However, energy considerations for a cooling flow suggest that T_{max} is somewhat smaller than T_{vir}. As discussed in § 3.1, an isobaric cooling flow releases an energy of $5/2kT_{max}$ per particle, $1kT_{max}$ of which comes from the pressure work required to compress the gas. Because only an energy of $3/2kT_{vir}$ is available at the inner disk edge, one might expect that $T_{max} = 3/5T_{vir}$. For the majority of objects in our sample, the data are consistent with $T_{max}/T_{vir} \leq 3/5$.

Several processes can lead to a reduced maximum temperature in an optically thin boundary layer. If the X-ray–emitting gas is rotating with a significant velocity, not all of the kinetic energy has been dissipated when the plasma begins to radiate, and T_{max} will be reduced. It is also possible that a significant amount of heat is conducted away from the hottest regions of the boundary layer before the plasma can radiate efficiently in X-rays. However, heat conduction does not dominate over cooling via X-ray emission, since otherwise T_{max} would be much smaller than T_{vir}. Furthermore, some of the accretion energy could be carried away in a wind, which would reduce the energy available to heat the remaining gas.

4.5. *Structure of the Boundary Layer*

The most striking result of our analysis is the excellent agreement of the X-ray spectra with a simple, isobaric cooling flow. This strongly suggests that the observed X-ray emission is produced by cooling plasma settling onto the white dwarf. The presence of a cooling flow has important implications for models of accretion in dwarf novae. In particular, it seems unlikely that a major fraction of the X-rays is emitted by an extended corona. If such a corona is present, its density must be too low for the emission of significant amounts of X-rays.

The high initial temperature of the cooling flow, which is close to the virial temperature (§ 4.4 and Fig. 8), indicates that the accreting gas in the boundary layer does not cool substantially until it has dissipated most of its rotational kinetic energy. It is apparent that the density in the upper parts of the boundary layer is insufficient for the emission of significant amounts of X-rays.

The results of our spectral analysis suggest the following picture of the boundary layer. At the inner disk edge, the accreting gas is decelerated well below the Keplerian velocity, and rotation can no longer support it against radial infall. The gas is accelerated toward the white dwarf, while it continues to lose angular momentum until most of its rotational kinetic energy has been dissipated. This dissipation heats the accretion flow to temperatures comparable to the virial temperature ($\geq 10^8$ K). The inward acceleration, as well as a vertical expansion of the boundary layer, caused by the large temperature increase, leads to a considerable drop in density. Because of the low density, the gas can no longer radiate efficiently and becomes invisible to us. Eventually, when the hot accretion flow begins to pile up on the white dwarf, the density increases rapidly, and the plasma begins to cool strongly via the emission of X-rays, while closely resembling an isobaric cooling flow. This picture of the boundary layer is in remarkable qualitative agreement with the model calculations by Narayan & Popham (1993) for dwarf novae at low accretion rates.

An alternative picture of the inner accretion disk is discussed in Meyer & Meyer-Hofmeister (1994). The authors suggest that the inner disk in quiescent dwarf novae becomes unstable and is evaporated by a coronal siphon flow. The gas in the forming corona is partially accreted onto the white dwarf and partially lost in a wind. If the density in the corona is low, the X-ray spectrum would be dominated by emission from the cooling plasma piling up on the white dwarf. This scenario is also consistent with the results of our spectral analysis.

The two pictures of the boundary layer discussed above are also supported by our timing analysis of VW Hyi data presented in Pandel et al. (2003). We discovered that the variations of the X-ray and the UV flux seen on a timescale of $\sim$1500 s are correlated and that the X-ray fluctuations are delayed with respect to the UV by $\sim$100 s. We attributed this correlation to accretion rate fluctuations that propagate from the inner disk to the X-ray–emitting part of the boundary layer. However, no such correlations were found for the other dwarf novae in our sample.

4.6. *Elemental Abundances*

The elemental abundances in the boundary layer are shown in Table 5. We obtained good constraints for O and Fe as these elements exhibit strong Lyα and Kα emission lines (Figs. 1–3). Somewhat less accurate are our abundance estimates for Ne, Mg, Si, and S, while only poor constraints were derived for C and N. Our results are mostly consistent with near solar abundances. One noticeable exception is the high nitrogen abundance in U Gem (see below). The oxygen abundances are consistently subsolar for the dwarf novae with an average value of $\sim$0.5 solar. For the low to moderate accretion rates during our observations, it is unlikely that significant mixing between the boundary layer and the white dwarf occurred. Our spectral analysis therefore measures the elemental abundances in the accreting matter, which are equal to the abundances on the companion star.

For two of the dwarf novae in our sample, the abundances in the white dwarf's photosphere have been determined from UV spectroscopic observations. Long & Gilliland (1999) analyzed white dwarf spectra of U Gem and found an overabundance of nitrogen at 4 times solar and an underabundance of carbon at 0.1 times solar. The authors explain these distinctly nonsolar abundances via accretion of material that has previously been processed by CNO burning, either in the core of a massive star or in a weak nova explosion on the white dwarf. From our spectral analysis of the U Gem data, we find similar nonsolar abundances in the accretion flow ($\sim$5 for nitrogen and $<$0.4 for carbon). This confirms that the origin of the unusual composition on the white dwarf is indeed accretion of material from a secondary with nonsolar abundances. Interestingly, none of the other objects in our sample show a similar overabundance of nitrogen. The unusual abundances on the secondary in U Gem may be the result of a more massive primary in the precataclysmic binary. During common envelope evolution, the composition of the secondary can be significantly altered by the mass transfer from the red giant primary. If the primary is massive enough to allow CNO burning, this contamination of the secondary could lead to unusual nitrogen and carbon abundances such as those observed in U Gem. A primary more massive than in most precataclysmic binaries is indicated by the comparatively high mass of the white dwarf in U Gem.

White dwarf photospheric abundances indicative of CNO burning were also found in VW Hyi (Sion et al. 2001, 1997). The authors interpreted this as evidence that a thermonuclear runaway has occurred on the white dwarf. Our spectral analysis of the *XMM-Newton* data did not reveal such distinctly nonsolar abundances in the boundary layer. This clearly demonstrates that the unusual abundances in VW Hyi are indeed a result of nuclear burning on the white dwarf and not accretion from the secondary.

Both a thermonuclear runaway on the white dwarf and accretion from the secondary could be responsible for the unusual abundances observed in some dwarf novae. An X-ray spectral analysis with a cooling flow model can be an important tool to measure the elemental abundances on the secondary and therefore distinguish between the two possibilities.

4.7. *EI UMa*

The spectrum of EI UMa differs significantly from those of the other objects in our sample (see § 3.3). The most distinctive features are the harder spectral slope, the weakness of Fe L-shell emission at 0.7–1.3 keV, the fluorescent Fe Kα line at 6.4 keV, and the strong O VII triplet at 22 Å. These spectral features are typically not seen in dwarf novae but appear to be prominent in intermediate polars. In a study of *Chandra* HETG spectra of four intermediate polars and three dwarf novae (Mukai et al. 2003), three of the intermediate polars exhibited the same distinctive spectral features as EI UMa (harder spectral slope, weak Fe L-shell lines, strong O VII lines), whereas the three dwarf novae had cooling flow spectra similar to the dwarf novae in our sample with strong Fe L-shell emission and only weak O VII lines. A prominent feature in the spectrum of EI UMa is the fluorescent Fe Kα line at 6.4 keV, which appears to be strong in magnetic cataclysmic variables (Ezuka & Ishida 1999) but is weak or absent for the nine dwarf novae in our sample. Because of the distinctive spectral features, we suspect that EI UMa is a magnetic cataclysmic variable of the intermediate polar type.

In the catalog by Ritter & Kolb (2003), EI UMa is classified as a U Gem–type dwarf nova. However, we were not able to find published results that support this classification, and we suspect that it is based solely on the nondetection of X-ray oscillations caused by the white dwarf rotation (Cook 1985). To our knowledge, no dwarf nova outbursts, which would justify this classification, have been observed. Thorstensen (1986) suggested that EI UMa may be a DQ Her star (intermediate polar) based on the X-ray characteristics and strong He II λ4686 (Green et al. 1982). We searched the *XMM-Newton* data for periodic oscillations that would identify EI UMa as an intermediate polar, but we could not find a clearly periodic signal in either the X-ray or the UV light curves. However, at periods longer than $\sim$100 s, the periodograms displayed strong spectral power due to the

flickering common in cataclysmic variables, which could mask small periodic oscillations. Since the orbital inclination of EI UMa is low ($\sim 23^\circ$; Thorstensen 1986), the accretion region is probably not occulted by the white dwarf, and the oscillation amplitude is likely to be small. If the white dwarf is rotating slowly (period > 100 s), periodic oscillations due to the white dwarf rotation may therefore be difficult to detect. In intermediate polars, there appears to be a rough correlation between the spin and orbital periods. For the 6.4 hr orbital period of EI UMa, the sample of intermediate polars in Warner & Wickramasinghe (1991) suggests a white dwarf spin period >2000 s. The duration of the two *XMM-Newton* observations (<10,000 s) is insufficient to detect small oscillations with such long periods. We therefore conclude that the nondetection of oscillations does not rule out the possibility that EI UMa is a magnetic system.

The strongest evidence for EI UMa being an intermediate polar is probably the low observed UV luminosity. As shown in Figure 4, EI UMa is the only object in our sample with a $L_{\rm UVW1}$ lower than predicted from the assumption of equal disk and boundary layer luminosities. It would be difficult to explain such a low $L_{\rm UVW1}$ if EI UMa were a dwarf nova. However, if EI UMa is an intermediate polar, the accretion disk is disrupted by the white dwarf's magnetic field, and the low UV luminosity is simply the result of a missing inner disk. We estimated the inner disk radius $R_{\rm in}$ with the relation $L_{\rm disk} = GM_{\rm wd}\dot{M}_{\rm bl}/R_{\rm in}$. Using a simple disk blackbody model to derive $L_{\rm disk}$ from $L_{\rm UVW1}$, we obtained an inner disk radius of $2.6R_{\rm wd}$ for the first and $2.0R_{\rm wd}$ for the second EI UMa observation. From a simple magnetic dipole model (e.g., Frank et al. 1992), we estimate a surface magnetic field strength of 1×10^4 G, which is at the lower end of field strengths in intermediate polars.

According to the standard model of the accretion column in magnetic white dwarfs, the shock temperature is directly related to the white dwarf mass (e.g., Wu 2000). With the assumption that the shock temperature is the same as the initial cooling flow temperature of ~ 50 keV (i.e., the postshock gas does not cool until it is dense enough to radiate efficiently in X-rays), we derive a white dwarf mass of 0.95 $M_\odot$. Here it was also assumed that the shock height is small compared to the white dwarf radius.

The presence of a partially covering absorber in EI UMa provides further support for our intermediate polar classification. Of the nine dwarf novae in our sample, only the eclipsing binary OY Car shows evidence of such an absorber. If EI UMa were a dwarf nova, its low orbital inclination of $\sim 23^\circ$ would make the presence of a partially covering absorber unlikely. For intermediate polars, however, partial absorption by the cool gas in the preshock accretion column is widely observed (e.g., Ezuka & Ishida 1999).

The equivalent width of ~ 110 eV of the fluorescent Fe Kα line at 6.4 keV is similar to those found in intermediate polars, which are typically around 100–150 eV (Ezuka & Ishida 1999). The likely origin of the fluorescent emission is the cool preshock accretion flow or the white dwarf's photosphere near the accretion region. Because the accretion flow is responsible for both the partial absorption and some of the fluorescence, one might expect a connection between the column density and the equivalent width of the fluorescent Fe Kα line. Using the method described in Ezuka & Ishida (1999), we estimate that the preshock flow contributes ~ 10 eV to the equivalent line width. However, this result is somewhat uncertain, since we only know the properties of the partial absorber along the line of sight. The fluorescent Fe Kα emission in EI UMa is probably dominated by the white dwarf. The calculations by George & Fabian (1991) for reflection off a circular slab of cold material predict an equivalent line width of 110 eV for a viewing angle of 60° with respect to the surface normal.

The strengths of the resonance (r), intercombination (i), and forbidden (f) lines of the O VII triplet at 22 Å (Table 4) can be used to determine the temperature and density in the region where oxygen is predominantly in a He-like ionization state. The line ratios widely used for He-like ions are $G = (f + i)/r$ and $R = f/i$ (e.g., Porquet & Dubau 2000 and references therein). For EI UMa these ratios are $G = 0.7$ and $R < 0.2$. The low value of G indicates that collisional ionization and not photoionization is the dominant process in the plasma. It also shows that the temperature of the gas emitting the O VII lines is >200 eV (see calculations in Porquet & Dubau 2000). The low R ratio (weak forbidden line) seems to suggest a high electron density $n_e \geq 10^{12}$ cm^{-3}. However, a low R ratio can also be caused by a strong UV radiation field. As shown in Mauche (2002), the radiation from a 30,000 K blackbody is sufficient for the R ratio of O VII to be in the high density limit, even if the density is low. Since the photosphere below the accretion column typically has temperatures this high, the R ratio cannot be used as a density diagnostic.

The origin of the strong O VII line emission is somewhat puzzling. The overall spectrum is well described by our cooling flow model, yet the integrated O VII line flux is about a factor of 10 larger than predicted by this model. One might suspect that the emission measure at the bottom of the accretion column, where temperatures are low enough for O VII to be the dominant ion, is larger than predicted by the cooling flow model. However, if this were the case, the temperature obtained from the G ratio (>200 eV) would imply a stronger O VIII Kα line than is actually observed.

We suspect that the O VII line emission originates from a transient plasma near the shock. A transient plasma can be present if the electron temperature is changed so quickly that the population densities of the different ionization states do not have enough time to reach their equilibrium values (for a discussion of transient plasmas see Liedahl 1999). Such a fast temperature change occurs at the accretion shock in magnetic cataclysmic variables. Before the shock, the accreting gas is cool, and oxygen is in a low ionization state. At the shock, the electron temperature rises quickly to several tens of kilo–electron volts, but the atoms remain in lower ionization states for some time before they can be ionized to O VIII. The X-ray spectral signature of such a transient plasma would be a continuum consistent with a high electron temperature and greatly enhanced O VII line emission.

In a transient plasma, O VII remains the dominant ionization state until a time t after the shock given by $n_e t \approx 10^{11}$ cm^{-3} s (Liedahl 1999). For a typical electron density $n_e \approx 10^{13}$ cm^{-3} (Mauche 2002), t is ~ 0.01 s. Since the postshock velocity is ~ 1000 km s^{-1} ($\frac{1}{4}$ of free-fall velocity), the region in which oxygen line emission is dominated by O VII extends to ~ 10 km or $\sim 0.002R_{\rm wd}$ below the shock. For a small shock height, this can be a significant fraction of the accretion column. We conclude that a transient plasma is a viable explanation for the strong O VII lines observed in EI UMa. With this interpretation it also becomes evident why the O VII line triplet is much weaker in dwarf novae where no single standoff shock is present. The many smaller shocks in the turbulent boundary layer of a dwarf nova heat the gas much more slowly than the standoff shock in a magnetic system. Note that in a transient plasma the He-like lines of elements other than oxygen should also be enhanced. However, we expect these He-like lines to be very weak, since we do not detect the Lyα lines of any elements other than oxygen in the RGS spectra.

5. CONCLUSIONS

Our spectral analysis of *XMM-Newton* data for eight quiescent dwarf novae revealed that the X-ray emission originates from a hot, optically thin multitemperature plasma. The temperature distribution in the plasma is in close agreement with an isobaric cooling flow, which points to a cooling plasma settling onto the white dwarf as the source of the X-rays. We found that the initial temperature of the cooling flow is comparable to the virial temperature. This is an indication that the accreting gas in the boundary layer does not cool substantially until it has dissipated most of its kinetic energy and begins to settle onto the white dwarf. We found that the X-ray–emitting gas in the cooler parts of the boundary layer is moving significantly slower than the inner accretion disk. This implies that the white dwarfs of all dwarf novae in our sample are rotating considerably slower than their breakup velocity.

Our findings are in qualitative agreement with the model calculations by Narayan & Popham (1993) for a disklike boundary layer. Conversely, the presence of an extended, X-ray–emitting corona can be excluded. With the new generation of X-ray telescopes, our observational knowledge of the boundary layer has reached a level of detail that needs to be matched by theoretical model calculations. Of special interest to the observer is the predicted distribution of emission measure versus temperature for the X-ray–emitting gas. In particular, it would be useful to know how theoretical predictions compare to the simple, isobaric cooling flow that appears to be the dominant source of X-rays in dwarf novae.

We found no evidence of an underluminous boundary layer in any of the eight quiescent dwarf novae, and our data are consistent with $L_{\rm disk} \approx L_{\rm bl}$ in all cases. For four of the dwarf novae, $L_{\rm disk}/L_{\rm bl} > 1$ can be clearly ruled out, whereas for the others an underluminous boundary layer could be present with $L_{\rm disk}/L_{\rm bl}$ ratios up to 2–4. Our findings disagree with those of van Teeseling & Verbunt (1994), who measured UV to X-ray flux ratios of 10 and higher. However, the authors did not consider the contribution from the white dwarf, which may dominate over the disk emission in the UV. Our results seem to suggest that there is no actual "mystery of the missing boundary layers" for the majority of quiescent dwarf novae. The key to understanding whether there really is a missing boundary layer problem is an accurate determination of the true disk luminosity.

We determined the elemental abundances in the boundary layer, which are likely equal to the abundances on the companion star. With a few exceptions, abundances are close to solar values. We have demonstrated on two of the dwarf novae that X-ray spectra can be used to identify the origin of unusual abundances on the white dwarf. We found that in VW Hyi the unusual abundances are the result of a thermonuclear runaway on the white dwarf, whereas in U Gem they were caused by accretion from the companion star. For most of the dwarf novae, absorption of boundary layer emission by the accretion disk does not appear to be important. Only for the eclipsing dwarf nova OY Car, which has a high orbital inclination of 83°, do we find evidence of a partially covering absorber.

The X-ray spectrum of EI UMa differs considerable from those of the other objects in our sample. The most distinctive features are the weakness of Fe L-shell emission, the strong fluorescent Fe Kα line, and the strong O VII line triplet. We also found that the disk luminosity is significantly lower than the X-ray luminosity. Our findings provide ample evidence that EI UMa is probably an intermediate polar and not, as previously thought, a U Gem–type dwarf nova. The high shock temperature of $\sim$50 keV indicates a white dwarf mass of $\sim 0.95\ M_{\odot}$. The strong O VII line triplet is possibly a result of a transient plasma below the shock. We have demonstrated that X-ray spectroscopic observations can be used to distinguish intermediate polars from dwarf novae.

This work is based on observations obtained with *XMM-Newton*, an ESA science mission with instruments and contributions directly funded by ESA member states and the USA (NASA). D. P. and F. A. C. acknowledge support from NASA grant NAG5-12390. We acknowledge with thanks the variable star observations from the AAVSO International Database, contributed by observers worldwide and used in this research.

REFERENCES

Anders, E., & Grevesse, N. 1989, Geochim. Cosmochim. Acta, 53, 197
Arnaud, K. A. 1996, in ASP Conf. Ser. 101, Astronomical Data Analysis Software and Systems V, ed. G. Jacoby & J. Barnes (San Francisco: ASP), 17
Bruch, A., Beele, D., & Baptista, R. 1996, A&A, 306, 151
Cash, W. 1979, ApJ, 228, 939
Cheng, F. H., Marsh, T. R., Horne, K., & Hubeny, I. 1994, in AIP Conf. Proc. 308, The Evolution of X-ray Binaries, ed. S. S. Holt & C. S. Day (New York: AIP), 197
Cook, M. C. 1985, MNRAS, 215, 81P
de Martino, D., Matt, G., Belloni, T., Haberl, F., & Mukai, K. 2004, A&A, 415, 1009
den Herder, J. W., et al. 2001, A&A, 365, L7
Ezuka, H., & Ishida, M. 1999, ApJS, 120, 277
Ferland, G. J., Pepper, G. H., Langer, S. H., MacDonald, J., Truran, J. W., & Shaviv, G. 1982, ApJ, 262, L53
Frank, J., King, A., & Raine, D. 1992, Accretion Power in Astrophysics (Cambridge: Cambridge Univ. Press), chapter 6.3
Gaensicke, B. T., & Beuermann, K. 1996, A&A, 309, L47
George, I. M., & Fabian, A. C. 1991, MNRAS, 249, 352
Green, R. F., Ferguson, D. H., Liebert, J., & Schmidt, M. 1982, PASP, 94, 560
Haberl, F., & Motch, C. 1995, A&A, 297, L37
Haberl, F., Motch, C., & Zickgraf, F.-J. 2002, A&A, 387, 201
Hamada, T., & Salpeter, E. E. 1961, ApJ, 134, 683
Hameury, J. M., & King, A. R. 1988, MNRAS, 235, 433
Harrison, T. E., McNamara, B. J., Szkody, P., McArthur, B. E., Benedict, G. F., Klemola, A. R., & Gilliland, R. L. 1999, ApJ, 515, L93
Hessman, F. V., Koester, D., Schoembs, R., & Barwig, H. 1989, A&A, 213, 167
Horne, K., Marsh, T. R., Cheng, F. H., Hubeny, I., & Lanz, T. 1994, ApJ, 426, 294
Ishida, M., Fujimoto, B., & Matsuzaki, K. 1996, in Cataclysmic Variables and Related Objects, ed. A. Evans & J. H. Wood (Dordrecht: Kluwer), 259
Jansen, F., et al. 2001, A&A, 365, L1
King, A. R. 1997, MNRAS, 288, L16
La Dous, C. 1991, A&A, 252, 100
Lasota, J. P., Hameury, J. M., & Hure, J. M. 1995, A&A, 302, L29
Liedahl, D. A. 1999, in X-Ray Spectroscopy in Astrophysics, ed. J. van Paradijs & J. Bleeker (New York: Springer), 189
Liedahl, D. A., Osterheld, A. L., & Goldstein, W. H. 1995, ApJ, 438, L115
Long, K. S., & Gilliland, R. L. 1999, ApJ, 511, 916
Long, K. S., Sion, E. M., Huang, M., & Szkody, P. 1994, ApJ, 424, L49
Lynden-Bell, D., & Pringle, J. E. 1974, MNRAS, 168, 603
Mahasena, P., & Osaki, Y. 1999, PASJ, 51, 45
Makishima, K., Maejima, Y., Mitsuda, K., Bradt, H. V., Remillard, R. A., Tuohy, I. R., Hoshi, R., & Nakagawa, M. 1986, ApJ, 308, 635
Mason, K. O., et al. 2001, A&A, 365, L36
Mauche, C. W. 2002, in ASP Conf. Ser. 261, The Physics of Cataclysmic Variables and Related Objects, ed. B. T. Gänsicke, K. Beuermann, & K. Reinsch (San Francisco: ASP), 113
Medvedev, M. V., & Menou, K. 2002, ApJ, 565, L39
Mewe, R., Gronenschild, E. H. B. M., & van den Oord, G. H. J. 1985, A&AS, 62, 197
Meyer, F., & Meyer-Hofmeister, E. 1994, A&A, 288, 175
Mitsuda, K., et al. 1984, PASJ, 36, 741
Mukai, K., Kinkhabwala, A., Peterson, J. R., Kahn, S. M., & Paerels, F. 2003, ApJ, 586, L77

Mukai, K., Wood, J. H., Naylor, T., Schlegel, E. M., & Swank, J. H. 1997, ApJ, 475, 812
Mushotzky, R. F., & Szymkowiak, A. E. 1988, in Cooling Flows in Clusters and Galaxies, ed. A. C. Fabian (Dordrecht: Kluwer), 53
Narayan, R., & Popham, R. 1993, Nature, 362, 820
Pandel, D., Córdova, F. A., & Howell, S. B. 2003, MNRAS, 346, 1231
Perna, R., McDowell, J., Menou, K., Raymond, J., & Medvedev, M. V. 2003, ApJ, 598, 545
Ponman, T. J., Belloni, T., Duck, S. R., Verbunt, F., Watson, M. G., Wheatley, P. J., & Pfeffermann, E. 1995, MNRAS, 276, 495
Porquet, D., & Dubau, J. 2000, A&AS, 143, 495
Ramsay, G., et al. 2001a, A&A, 365, L288
———. 2001b, A&A, 365, L294
Ritter, H., & Kolb, U. 2003, A&A, 404, 301
Shafter, A. W., & Szkody, P. 1984, ApJ, 276, 305
Sion, E. M. 1991, AJ, 102, 295
———. 1999, PASP, 111, 532
Sion, E. M., Cheng, F. H., Sparks, W. M., Szkody, P., Huang, M., & Hubeny, I. 1997, ApJ, 480, L17
Sion, E. M., Cheng, F. H., Szkody, P., Gänsicke, B., Sparks, W. M., & Hubeny, I. 2001, ApJ, 561, L127
Sion, E. M., Long, K. S., Szkody, P., & Huang, M. 1994, ApJ, 430, L53
Sproats, L. N., Howell, S. B., & Mason, K. O. 1996, MNRAS, 282, 1211
Strüder, L., et al. 2001, A&A, 365, L18
Szkody, P., Nishikida, K., Raymond, J. C., Seth, A., Hoard, D. W., Long, K. S., & Sion, E. M. 2002, ApJ, 574, 942
Thorstensen, J. R. 1986, AJ, 91, 940
Turner, M. J. L., et al. 2001, A&A, 365, L27
Tylenda, R. 1981, Acta Astron., 31, 127
van Teeseling, A., Beuermann, K., & Verbunt, F. 1996, A&A, 315, 467
van Teeseling, A., & Verbunt, F. 1994, A&A, 292, 519
Verbunt, F. 1987, A&AS, 71, 339
Wade, R. A. 1982, AJ, 87, 1558
Warner, B. 1987, MNRAS, 227, 23
———. 1995, Cataclysmic Variable Stars (Cambridge: Cambridge Univ. Press)
Warner, B., & Wickramasinghe, D. T. 1991, MNRAS, 248, 370
Wheatley, P. J., & West, R. G. 2003, MNRAS, 345, 1009
Wu, K. 2000, Space Sci. Rev., 93, 611